10.1098/rsta.2003.1326

THE ROYAL SOCIETY

All-optoelectronic continuous-wave terahertz systems

By Torsten Löffler, Karsten J. Siebert, Holger Quast, Noburu Hasegawa, Gabriel Loata, Robert Wipf, Tobias Hahn, Mark Thomson, Rainer Leonhardt and Hartmut G. Roskos

Physikalisches Institut, Johann Wolfgang Goethe-Universität, Robert-Mayer-strasse 2–4, 60054 Frankfurt-am-Main, Germany
(t.loeffler@physik.uni-frankfurt.de)

Published online 17 December 2003

We discuss the optoelectronic generation and detection of *continuous-wave* terahertz (THz) radiation by the mixing of visible/near-infrared laser radiation in photoconductive antennas. We review attempts to reach higher THz output-power levels by reverting from mobility-lifetime-limited photomixers to transit-time-limited p-i-n photodiodes. We then describe our implementation of a THz spectroscopy and imaging-measurement system and demonstrate its imaging performance with several examples. Possible application areas of THz imaging in the biomedical field and in surface characterization for industrial purposes are explored.

Keywords: lasers; THz radiation; THz imaging

1. Introduction

The controlled, direct generation of electromagnetic radiation in the terahertz (THz) frequency regime (100 GHz–10 THz) is a challenging task. The main reason for this is the fact that electronic methods on the low-frequency side are limited to some hundreds of GHz (Rodwell *et al*. 2001). On the other side, optical methods either require bulky and expensive machinery (free-electron or molecular-gas lasers) or are hampered by the need for cryogenic operation conditions (p-Ge laser, quantum cascade laser (Köhler *et al*. 2002)). An alternative approach is the optoelectronic generation of THz radiation by nonlinear photomixing (down-conversion) techniques. These were first developed on the basis of pulsed laser systems delivering radiation in the visible or near-infrared spectral range (Johnson & Auston 1975). The conversion to THz frequencies was (and is) achieved by the excitation of photocurrent pulses in semiconductor devices which act as the source for THz pulses.

Of prime importance for the development of the THz research field were the facts that photoconductive antennas can also be employed as detectors for the THz radiation and that the detected physical quantity is the electric radiation field vector and not the intensity. The latter aspect in conjunction with lock-in averaging is the reason for a very high receiver sensitivity and an exceedingly efficient suppression

One contribution of 16 to a Discussion Meeting 'The terahertz gap: the generation of far-infrared radiation and its applications'.

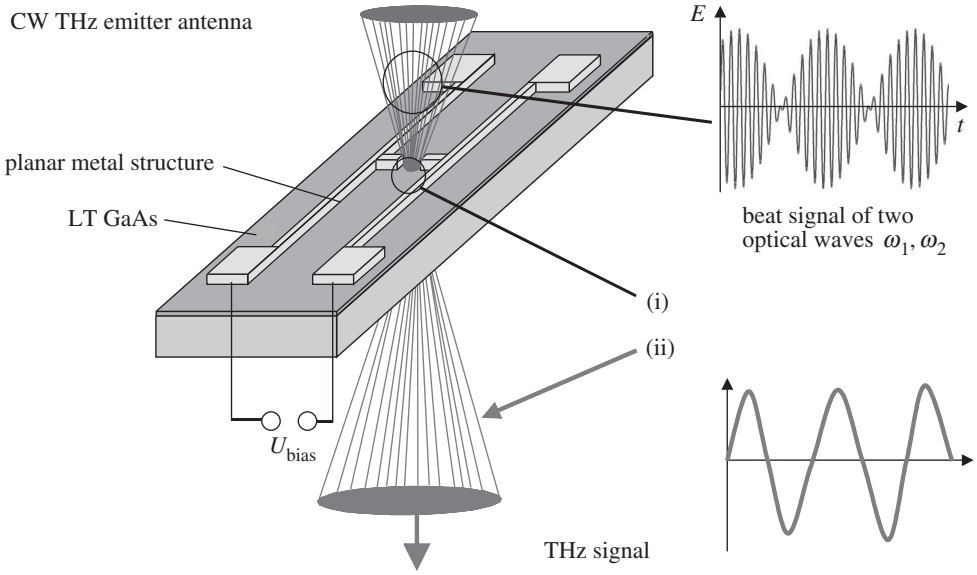

Figure 1. Photoconductive H-dipole antenna for the generation of CW THz radiation by the mixing of two visible/near-infrared laser beams. (i) $I_{\mathrm{photo,AC}} \propto U_{\mathrm{bias}} P_{\mathrm{opt}} \sin(\omega_{\mathrm{diff}} t)$; (ii) $P_{\mathrm{THz}} \propto I^2_{\mathrm{photo,AC}}$.

of the thermal background radiation. The background—in contrast to the useful radiation—has an ultra-rapidly fluctuating orientation of the electric field vector which leads to efficient averaging-out of the equally fluctuating photocurrents it generates in the receiver which can be kept (as well as the emitter) at ambient temperature. Another advantage of THz optoelectronics is the phase sensitivity, which arises by the stroboscopic detection principle. The capability to measure both the amplitude and the phase of the electric radiation field allows us to determine the complex refractive index of a material brought into the THz beam path.

The optoelectronic approach indisputably has revolutionized the application of THz radiation in physics and (to a lesser but nowadays rising degree) in other research fields (Roskos 1996). So far, however, these exciting developments have not led to spin-offs into industrial applications. The key reasons (besides the delaying effects of educational and training aspects) seem to be that the femtosecond lasers at the heart of the advanced THz systems remain expensive and bulky, and that the optical-to-THz power conversion efficiency is low (not exceeding 10^{-4}) necessitating continuously good alignment of the complex measurement system and rendering large-area imaging time-consuming (see below). For these reasons, there is an interest in finding conceptual alternatives without giving up the advantages of the coherent detection scheme discussed above, namely the capability to measure both the amplitude and phase of THz signals over a large frequency range (several THz) with high signal-to-noise ratio (SNR).

A number of years ago, it was recognized that photomixing of two *continuous-wave* (CW) laser beams holds much promise to overcome the first of the two fundamental limitations for an industrialization of optoelectronic THz technology. This is because compact and inexpensive CW semiconductor lasers with high output power and stable monomode operation are gradually becoming accessible for mixing applications.

The THz frequency and line width being essentially pre-selected by the choice of the laser wavelengths and line widths, CW mixing offers the additional opportunity to build narrow-line-width sources as they are wanted for local-oscillator purposes and high-resolution spectroscopy. After its first demonstration by Brown *et al.* (1993*a*, *b*), mixing of the radiation of much more compact semiconductor lasers has been investigated by a number of groups (Brown *et al.* 1994, 1995; McIntosh *et al.* 1995; Matsuura *et al.* 1997, 1999; Verghese *et al.* 1998; Gu *et al.* 1999). The first implementation of an all-optoelectronic THz measurement system was demonstrated in 1998 by Verghese *et al.*, who employed the optical-beat signal from two CW Ti:sapphire lasers operating at different wavelengths, in order to generate and detect the THz signal with photoconductive antennas (Verghese *et al.* 1998). A short time later, electro-optic detection (Wu *et al.* 1996; Chen *et al.* 2000; Han *et al.* 2000), a technique well established for pulsed THz systems, was also introduced in a CW system (Nahata *et al.* 1999). Recently, THz imaging based on CW optoelectronic systems has been demonstrated employing either a photoconductive receiver (Siebert *et al.* 2002*a*, *b*) or electro-optic detection (Nahata *et al.* 2002).

In the following, we provide an overview on the state of the art in photomixer development, discuss several approaches to enhancing the THz output power and introduce CW optoelectronic THz imaging.

2. State-of-the-art photoconductive antennas

A simple example of a photoconductive antenna for the optoelectronic generation (detection) of CW radiation around and above 1 THz is shown in figure 1. Like its counterpart for THz pulses, it consists of a metallic radiative structure (here an H-shaped dipole) with feed lines and a photoconductive gap (photoswitch) with an area of typically 50–100 μm^2. At present, one employs almost exclusively low-temperature-grown GaAs (LT GaAs) as the photoswitching material. Compared with antennas for pulsed operation, one optimizes a CW photoconductive antenna essentially in the same way with respect to the LT-GaAs properties, but differently with respect to the antenna design and the avoidance of parasitic influences by the GaAs substrate and the metal environment.

Concerning the LT-GaAs properties (Tani *et al.* 1994; Jackson *et al.* 1999), the optimization potential results from the dependence of the output power P_{THz} on the following parameters: F_{opt}, the optical fluence in the photoswitch; R_{ant}, the impedance of the antenna; $I_{\mathrm{photo,DC}}$, the generated DC photocurrent; E_{bias}, the applied DC bias field; μ, the mobility of the photogenerated carriers in the LT-GaAs material; and τ, the mobility lifetime. The output power (neglecting the RC time constant limitation) is given by (Brown *et al.* 1993*a*; Matsuura *et al.* 1997)

$$P_{\mathrm{THz}}(F_{\mathrm{opt}}, \omega_{\mathrm{THz}}) = R_{\mathrm{ant}} \frac{1}{2} \frac{(I_{\mathrm{photo,DC}}(F_{\mathrm{opt}}))^2}{1 + \omega_{\mathrm{THz}}^2 \tau^2} \propto F_{\mathrm{opt}}^2 E_{\mathrm{bias}}^2 \frac{\tau^2 \mu^2}{1 + \omega_{\mathrm{THz}}^2 \tau^2}. \tag{2.1}$$

Here, ω_{THz} denotes the angular THz frequency (difference frequency of the optical waves). Equation (2.1) illustrates some important properties of the photoconductive antennas.

(i) The THz output power is proportional to the square of the DC photocurrent, as has also been verified experimentally (Brown *et al.* 1994). The THz output

power shows a frequency roll-off of the form $1/(1+\omega_{\mathrm{THz}}^2\tau^2)$. Thus, even for the shortest achievable mobility lifetime of *ca.* 0.2 ps, the 3 dB point does not exceed 1 THz.†

(ii) The maximum DC photocurrent and the related maximum output power for a given THz frequency are determined by both the operation conditions (F_{opt} and E_{bias}) and the material properties (μ and τ). Thus, for high output power, one chooses a material with a high value of μ and drives the device at such operation conditions as can be applied without device damage. With respect to τ, one has to go for the lowest value possible if the antenna is operated at and above 1 THz, but one can increase the output power by employing material with increased τ if the operation frequency is below 1 THz.

The control of both the mobility and the mobility lifetime are possible within limits by the growth and annealing conditions of the LT GaAs. One finds that the value of τ increases with both the growth and the annealing temperatures (Tani *et al.* 1994; Segschneider *et al.* 2002). On the other hand, reports on the behaviour of the mobility as a function of these temperatures do not give a consistent picture which may be due to the different measurement techniques applied to deduce the mobility (Segschneider *et al.* 2002; Němec *et al.* 2001; Stellmacher *et al.* 1999), an issue which requires clarification in the near future. Equally open is the question of whether the carrier lifetime (and the photocurrent) can be enhanced by very high bias fields, as has been reported in the literature (Zamdmer *et al.* 1999). Verghese *et al.* (2001) could not corroborate these findings.

With respect to the antenna design, one has much more flexibility to optimize emitters of CW radiation than those of pulsed radiation. While pulsed radiation favours the simplest radiative structures such as dipoles (Cai *et al.* 1997) or edge emitters (Zhao *et al.* 2002) (the simplicity of the radiator avoiding dispersive effects which result in complex and difficult-to-analyse pulse profiles), CW radiation can be generated with various types of radiating structures such as dipoles (Matsuura *et al.* 1997), logarithmic spirals (Brown *et al.* 1995), bow-ties (Tani *et al.* 1997) and double dipoles (Duffy *et al.* 2001), etc., thus optimizing not only the output power with the (frequency-dependent) quality factor of the resonator, but also the spatial radiation profile and the integration of the emitter into specific environments. Filter structures in the feed lines can keep power in the emitter which otherwise would be transmitted to the contacts and be lost. Such measures clearly can only be taken if the emitter is dedicated for a fixed frequency or a narrow frequency range.

An aspect requiring much attention when generating CW radiation is the undesired back-coupling from the environment and the substrate. With THz pulses, this feedback is insignificant, except in narrow-band applications, because it always delivers delayed signals which can be removed by time gating. This option does not exist when dealing with CW radiation, and hence back-coupling is as much of a problem here

† It should be noted, however, that THz pulses with a frequency content of up to 40 THz have been generated in specially designed photoconductive antennas (Kono *et al.* 2001). While the radiation up to a few THz is emitted by the radiative metal structure, the signals at very high frequencies most likely originate from both real and virtual (nonlinear electro-optic mixing) photocurrents in the LT GaAs, bypassing the metal structure. There is no obvious reason why one should not also reach such high frequencies in CW operation.

as in high-frequency CW electronics. The filters in the feed lines mentioned above help to prevent back-coupling at least from the circuitry surrounding the emitter.

A quite different problem of CW THz optoelectronics is imposed by the substrate of the LT-GaAs layer. If the substrate can absorb the residual optical radiation penetrating through the LT GaAs, there is the risk that photo-generated and long-lived charge carriers partly screen the applied bias field, a process clearly detrimental to the THz output power. This is an effect which is generally not found in pulsed THz systems because the charge carriers recombine fast enough before the next optical pulse arrives at the photomixer. At present, studies are underway to quantify the field-screening effect by carriers in the substrate of CW emitters.

The highest output powers reported in the literature are 2 μW at 1 THz and 150 nW at 2.5 THz (Duffy *et al.* 2001). In order to achieve these values, bias fields of more than 100 kV cm^{-1} and optical fluences of 10^5–10^6 W cm^{-2} (beam power of up to 100 mW on a photoswitch of $5 \times 5\,\mu\text{m}^2$) are required, producing DC photocurrents of up to 2 mA. Comparing the THz output power at 1 THz with that of high-repetition-rate pulsed sources (Zhao *et al.* 2002), one finds that the pulsed sources reach a time-averaged power roughly a factor of 10 higher. This power, however, is distributed over a large frequency range (0–4 THz). If spectral power density is of concern, the CW sources are clearly superior; if the field amplitude is relevant, however, pulsed sources prevail (with a 100 MHz Ti:sapphire laser source, one can generate peak electric fields in the focus of a THz beam of a few tens of volts per centimetre, while 1 μW of CW radiation at 1 THz produces a field of 1 V cm^{-1} within a diffraction-limited focus).

3. Novel concepts for optoelectronic CW THz generation

The maximum power which can be generated with current-driven antennas is given by the term

$$P_{\text{THz}} = \tfrac{1}{2} R_{\text{ant}} I_{\text{AC}}^2.$$

Novel concepts hence seek to increase either the antenna impedance R_{ant} or the AC current I_{AC} in the mixer element of the device.

A concept for an antenna with an increased impedance has recently been proposed by Sydlo *et al.* (2002). The basic idea is to reduce the influence of the permittivity of the substrate by fabricating the antenna on a thin membrane. A further increase in the impedance to more than 1.2 kΩ can be achieved in a narrow range around the design frequency by a backside metallization placed at a distance of 40 μm below the antenna.

Other interesting ideas pertain to an increase in the AC current amplitude in the photomixer. One should bear in mind that the AC current in standard photoswitches is determined by the applied bias voltage and the incident optical power which are both limited by damage thresholds. Several novel approaches concentrate on accommodating a higher optical power by distributing it over an extended mixer area typically embedded into electric waveguide structures. If the dimensions of the mixer element become larger than the wavelength of the generated THz wave, it is necessary to achieve phase matching of the impinging optical radiation and the generated THz wave. The literature reports two basic design forms. Both are based on coplanar transmission lines containing the photoconductive switch in the area between the metal stripes. In the first design (Matsuura *et al.* 1999), the waveguide

is illuminated from the top with two optical beams focused by cylinder lenses and tilted with respect to each other in order to form a standing-wave pattern which propagates with the same phase velocity as the THz wave guided along the transmission line. Instead of free-space illumination, the second approach (Duerr *et al.* 2000) employs excitation of the photoswitch from an optical waveguide positioned directly under the coplanar transmission line. Phase-matching is achieved by slowing down the THz wave with the help of filter elements incorporated into the transmission line. At present, none of the investigations has succeeded in demonstrating a higher THz output power at 1 THz than that obtained from the spot-illuminated sources addressed above. The limiting factors seem to be the THz signal losses in the metal of the coplanar transmission lines and in the substrate (free-carrier absorption). When these attenuation factors are under better control, waveguide approaches are likely to play an increasingly significant role as the available optical power rises.

In all of these devices, LT-GaAs is employed as photomixer material. With the low mobility lifetime restricting the achievable photocurrent, several other approaches attempt to overcome this limitation by reverting to transit-time-limited device structures of the p-i-n-photodiode type. In principle, such devices can exhibit a quantum efficiency close to 100%, yielding very high AC currents (one estimates a photocurrent of 70 mA if 800 nm laser radiation with an input power of 100 mW is fully absorbed in the photomixer). The problem is, however, to reconcile the high quantum efficiency with ultrahigh-speed operation. The former requires a sufficient thickness and width of the diode, while the latter is optimized by shrinking all dimensions—the thickness to keep the transit time short and the width to reduce the capacitance of the device.

An optimized realization of such a device is the so-called *unicarrier travelling photodiode* (UCT-PD) of the Nippon Telegraph and Telephone Corporation (NTT) for the 1.55 μm wavelength regime (Hirata *et al.* 2002; Ueda *et al.* 2003). It takes advantage of the very high mobility of electrons in InP-related materials. The photocarriers are generated in an absorption layer of p-type InGaAs close to the cathode. While the low-mobility holes are collected at this contact, the electrons are transferred to an InP drift layer of sufficient thickness to keep the device capacitance low enough. Operation frequencies of several hundred GHz have been tested. At 100 GHz, an output power of 2.2 mW at a photocurrent of 20 mA (with an optical input power of 100 mW) is achieved. At 1 THz, the output power extrapolates to a few microwatts (Hirata *et al.* 2002) indicating a strong roll-off which limits the THz frequency performance of the device.

In order to make p-i-n concepts attractive at 1 THz and above, there is no way around reducing the carrier transit time further. As this makes it unavoidable to go for ultrathin layers, one seems to run into unsolvable conflicts with the need for a sufficient absorber thickness and an ultralow device capacitance. Döhler *et al.* have recently proposed to ease the problem by adopting an approach with a stack of specially designed nano-p-i-n-diodes forming what they call a n-i-p-n-i-p-*hetero-superlattice* (Renner *et al.* 2002; Eckardt *et al.* 2003). Its first realization has been in the GaAs/AlGaAs material system (see figure 2). The absorption and the carrier drift in each period take place in the intrinsic (i) region, which consists of $Al_xGa_{1-x}As$ with a continuously changing Al content. With light at a wavelength of 850 nm, electron–hole generation occurs only in the region of lowest bandgap (lowest Al content) close to the p-layers. The photocurrent is mostly due to the electrons

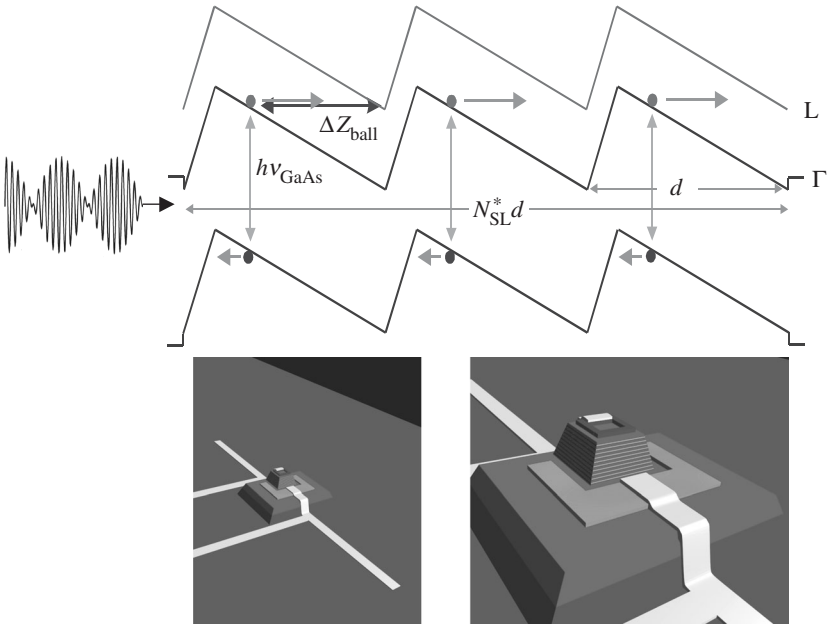

Figure 2. Top, scheme of the GaAs n-i-p-n-i-p superlattice showing three periods of the stack of layers with no external bias field applied. The lines display the band edges of the valence band and of the fundamental (Γ-valley) and the lowest side valley (L-valley) conduction band. Note that the intrinsic layer (lines tilted downwards) consists of $Al_xGa_{1-x}As$ with a continuously increasing Al content in each period. This produces an absorption region on the left side of each intrinsic layer, electrons drift to the right, holes to the left. Bottom: n-i-p-n-i-p structure embedded into a dipole emitter. ($\lambda_1 \approx \lambda_2 \approx 850$ nm, $\Delta\lambda \approx 2.4$ nm (~ 1 THz).)

which traverse the i-layer quasi-ballistically. The built-in fields are such that transfer of the electrons into the large-effective-mass L-valleys is avoided. The thickness of the i-layer is adjusted to the target operation frequency of the device (Δz_{ball} in figure 2 corresponding to the maximum distance over which an electron can propagate quasi-ballistically during half the oscillation period). The charge carriers are removed by recombination either at the contacts or at the interfaces between the p-layers and the n-layers (Pohl *et al*. 2003), the latter containing very thin LT-GaAs or ErAs layers to enhance carrier recombination.

An interesting property of the device is the possibility to achieve impedance matching of the mixer with the antenna simply by choosing the proper number N of the superlattice periods (Eckardt *et al*. 2003). For a target frequency of 1 THz, a drift length Δz_{ball} of 250 nm, and a device cross-section of 80 μm^2, one matches the antenna impedance of 70 Ω if N is chosen to be 10. Simulations suggest that the impedance matching should allow us to achieve a THz output of 500 μW upon illumination with 100 mW of absorbed laser power, i.e. a factor of 100 (250) more than theoretically expected (experimentally achieved) with single-spot LT-GaAs photomixers. Very recently, we have performed the first preliminary THz emission studies with non-optimal n-i-p-n-i-p photomixers, achieving immediately a conversion efficiency comparable to that of our best conventional LT-GaAs photoconductive antennas, which confirms the great potential of the n-i-p-n-i-p devices (Loata *et al*. 2003).

4. CW THz imaging

One of the most promising fields of applied THz research pertains to imaging and sensing. Since its first demonstration by Hu & Nuss (1995), optoelectronic THz imaging and sensing has become a rapidly expanding field of research (Mittleman *et al.* 1999; Herrmann *et al.* 2000). The potential for interesting applications such as in package inspection, security monitoring, process control, and biomedical or pharmaceutical imaging and sensing has been demonstrated (Woodward *et al.* 2001; Arnone *et al.* 2000; Arnone 2000; Mittleman *et al.* 1997). The developments have reached a maturity which allows the adaption of more sophisticated imaging techniques known from the optical region of the spectrum, e.g. near-field (Hunsche *et al.* 1998; Wynne & Jaroszynski 1999) and dark-field imaging (Löffler *et al.* 2001, 2002; Hasegawa *et al.* 2003), and microscopic imaging (van der Valk & Planken 2002; Chen *et al.* 2003). A viable technology for industrial use, however, is still lacking.

Almost all of the work was performed based on pulsed THz imaging systems. Although this technique has certain advantages such as the absolute-time-of-flight measurement capability and the access to the full spectral information within one measurement, there are a few drawbacks to be considered (in addition to the more general ones such as laser costs and complexity). On the system side, this is the need for a fast mechanical delay line to operate around the time-delay-zero point (shaker). This device limits the state-of-the-art systems to data-acquisition times of *ca.* 20 ms. A further improvement of mechanical shakers seems to be conceptually impossible. In addition, such a fast-moving delay line introduces mechanical vibrations, which create a host of problems not only in applications such as THz microscopy. On the application side, the pulsed systems are limited to a certain spectral resolution, which is given by the length of the time window scanned through at each pixel.

CW techniques, in contrast, allow for a more or less continuously running delay line (with the ensuing drastic reduction of the vibrations) and offer a high spectral purity. This and the enormous reduction which the implementation of semiconductor-laser-based systems will bring in terms of costs and complexity led us to develop the first all-optoelectronic CW THz imaging system (Siebert *et al.* 2002*a*, *b*).

Figure 3 shows the layout of our system. Two optical waves, with independently tunable wavelengths centred around 800 nm, are generated in a dual-colour CW Ti:sapphire laser (Siebe *et al.* 1999) consisting of two unidirectional, single-longitudinal-mode ring cavities sharing a single Ti:sapphire gain medium which is pumped by two beams from a 5 W Verdi all-solid-state laser (Coherent Inc., Santa Clara, CA, USA). The Ti:sapphire laser source will in the future be replaced by high-power semiconductor diode lasers, optionally in combination with an amplifier. For the research described here, the Ti:sapphire source has turned out to be a versatile and robust tool providing more than sufficient laser power and stable laser operation.

The emitted laser beams are spatially combined at a 50/50 beam-splitter cube yielding two beams which are intensity-modulated at the difference frequency of the optical waves. The subsequent optical system is similar to that of femtosecond-laser-based THz transmission-measurement systems. One of the optical beams is guided via a computer-controlled optical delay line to the emitter antenna; the other is used to gate the receiver antenna. We employ two H-shaped photomixer antennas both with a 50 μm long dipole and a $5 \times 10\ \mu m^2$ photoconductive gap on LT GaAs grown at 270 °C (emitter) and 200 °C (detector), respectively, exhibiting measured carrier

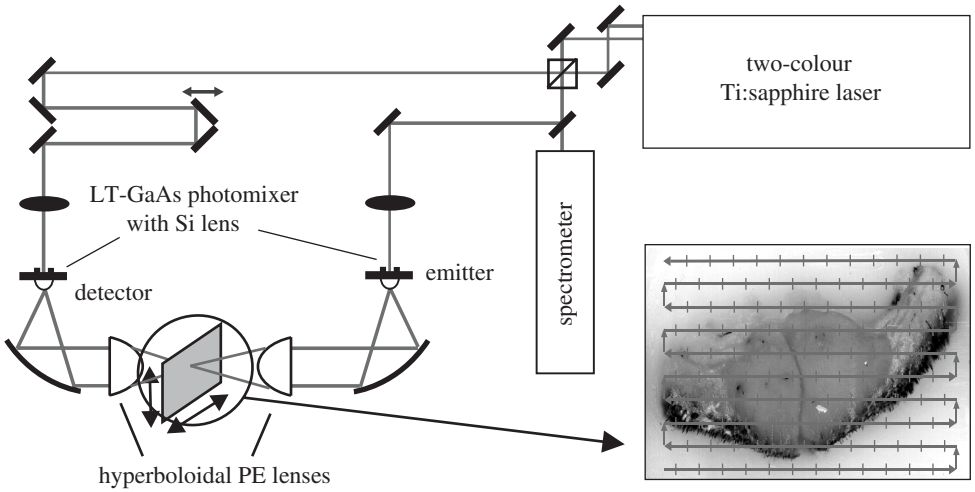

Figure 3. Schematic of the all-optoelectronic CW THz imaging system.

trapping times of 1.2 ps (emitter) and 0.35 ps (detector). The variation of the growth temperatures allows one to achieve higher output power from the emitter and broader detection bandwidth at the detector. Each photomixer is illuminated with 100 mW of optical power. The emitter is biased with a 25 kHz square-wave signal between ± 12.5 V. This modulation allows lock-in detection of the THz signal, while avoiding detrimental feedback into the two-colour laser source, which is found to occur when the optical beam is mechanically chopped. The lock-in time constant is set to 20 ms.

The THz radiation is coupled out of the emitter via a hyperhemispherical Si substrate lens of diameter 2 mm, collimated by an off-axis paraboloidal mirror and focused by a plano-hyperboloidal lens. It is then passed through the sample and guided onto the detector antenna with the reverse sequence of optics. The SNR obtained at 1 THz without a sample in the beam path is 100:1. The SNR is defined in terms of the mean amplitude versus its standard deviation.

For THz imaging, the sample is mounted on a computer-controlled x–y translation stage and can be moved continuously along a meandering path through the focus of the THz beam, as indicated in figure 3. The relative phase of the THz signal is varied by simultaneous translation of the optical delay line. In order to obtain the shortest possible data-acquisition time for the imaging system, we take advantage of the extremely long coherence length of the two optical single-longitudinal-mode beams. During the spatial scan over a horizontal row of the object, the optical-delay line is moved with constant velocity without changing its direction. For each pixel of the image, the phase of the detected THz wave is varied over two THz periods. Twelve temporal data points per period are sampled and employed for the evaluation of both the amplitude and phase of the sinusoidal THz field. At the end of each row of pixels, both the time-delay translation stage and the object's horizontal translation change directions simultaneously, while the object is moved to a new vertical position. For each object, a reference scan of the time delay is taken without the sample or at a transparent point on the sample, covering the same optical path length as during a scan of a row of pixels. It is taken in both forward and backward directions to

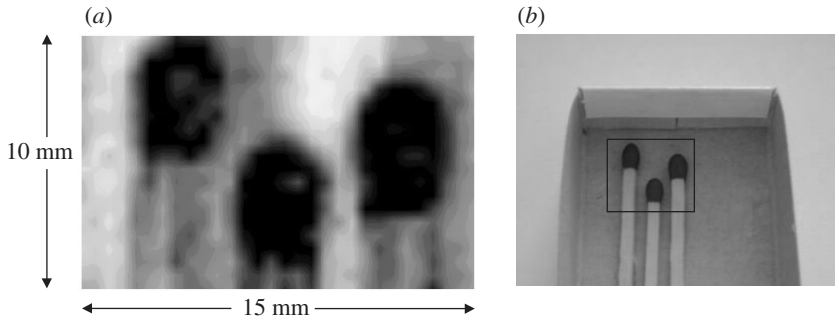

Figure 4. (*a*) THz transmission image of three matches in a closed box (view into a matchbox at 500 GHz, 600 pixel). (*b*) Photograph of the opened box with the matches inside.

compensate for any differences in the phase of the signal due to the change of the scanning direction.

In addition to the amplitude information, the relative phase of the CW wave at each pixel can be exploited for image formation (examples are not shown here; see Siebert *et al*. (2002*a*) for more details). For thin samples where the optical thickness varies by less than one wavelength, or for samples with a sufficiently homogeneous optical thickness (i.e. without changes larger than one wavelength) and a constant geometrical thickness, this information is equivalent to that obtained by time-of-flight measurements with pulsed systems. For samples with larger variations in the optical thickness, the modulo 2π ambiguity has to be taken into account.

With a routinely achieved data-acquisition time of 200 ms per pixel, our CW THz imaging system is at present about one order of magnitude slower than the best femtosecond-laser-based systems. We expect to reach the same or (with electronic instead of mechanical phase-shifters) even better acquisition times in the future. The images are of comparable quality (Siebert *et al*. 2002*a*; Teravision 2003). Single-scan measurements at 1 THz give SNRs better than 100:1 and allow for imaging with a dynamic range in power of more than three orders of magnitude. The spatial resolution is about one wavelength. With the same antennas, the system is suited to recording images in the region between 0.2 THz and 1.5 THz.

5. Imaging applications

(*a*) *Package inspection*

The observation that paper, cardboard, many plastic materials and a variety of other materials are quite transparent to THz radiation suggests its use for the inspection of containers, envelopes and packages made out of these materials. For illustration, figure 4 shows an image of some matches taken with our CW THz imaging system through the closed cardboard matchbox.

For industrial applications, one faces the problem that data-acquisition times of 20 ms (pulsed) or 200 ms (CW) are far too long for online two-dimensional imaging as required for, for example, security scans at airports or in mail-processing centres. A more realistic and less challenging task is one-dimensional imaging. This limited approach may be sufficient for some practical purposes such as the monitoring of the presence/lack of a substance in a package. In the food-processing industry, an

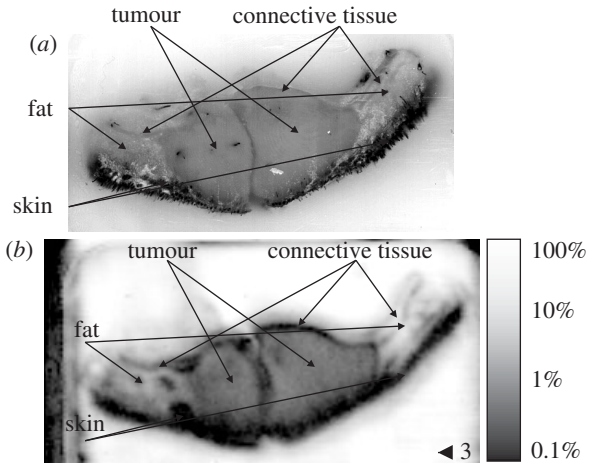

Figure 5. (*a*) Photograph of an archived tissue sample of a cut through a canine skin tumour. (*b*) CW THz transmission image of the sample.

example for such a task could be the test of the presence of raisins in cereal boxes. The raisins will give a good contrast due to their high water content.

If one is not bound to perform online imaging, one can take advantage of the phase sensitivity of optoelectronic THz sensing for more sophisticated applications such as three-dimensional imaging. It can be oriented towards remote surface reconstruction or aim at a tomographic analysis of the interior of a transparent object as has recently been demonstrated with a pulsed THz system (Ferguson *et al*. 2002). Conceptually, such THz tomography should also be possible with CW THz radiation.

(*b*) *Biomedical imaging*

THz imaging in the biomedical field attracts much interest (Knobloch *et al*. 2001; Fitzgerald *et al*. 2002; Woodward *et al*. 2001; Smye *et al*. 2001), one reason being the fact that THz radiation is non-ionizing and hence cannot—at the power levels employed in the submilliwatt regime—induce biochemical modifications in tissue that could be hazardous to living beings, as is the case with X-rays. We do not dwell further on fundamental aspects (such as the problem of the strong absorption of water in the THz frequency range), as here we only want to illustrate the imaging capability of CW THz radiation in the biomedical field, emphasizing that scattering and diffraction such as that in ultrasonic imaging can be employed advantageously as major contrast-forming mechanisms.

We show exemplarily an image taken from an archived (formaline-fixed, dehydrated and wax-mounted) slice through a canine skin tumour (basal cell tumour, see figure 5*a*). The size of the sample was 32 mm × 24 mm × 3 mm. Figure 5*b* shows a logarithmic power-transmission image taken with the CW system at 1 THz in a single meandering pass. The image consists of 11 248 pixels, corresponding to a separation of neighbouring pixels of 250 μm. The scan took 39 min, with a measurement time of 200 ms per pixel plus a short time at the end of each row to switch to the next one, and the 30 s required for the one-time reference scan. All different tissue parts of the sample can be identified. While it is not clear at present whether spectroscopic resonances play a major role in the formation of the image contrast, one

can clearly attribute the pronounced attenuation at the boundaries between different tissue types to scattering and diffraction effects. This was examined in detail and the effect augmented by THz dark-field measurements (Löffler *et al*. 2001, 2002).

(*c*) *Industrial surface inspection*

Besides the very popular fields of biomedical and security-related research, one should not neglect more traditional application areas where THz imaging and sensing may well have its first major impact in the industrial world. We have already addressed package control and tomography above. In this subsection, we point out that interesting applications could lie in quality control and process monitoring.

We have recently begun to examine the conceptual applicability of THz imaging and sensing for the inspection of the surfaces of rolled steel and other metals. These investigations aim at the online monitoring task of identifying small surface defects like protrusions, scratches and voids with vertical dimensions from a few micrometres to hundreds of micrometres and lateral dimensions in the millimetre range. In the case of steel, the protrusions and voids may originate from air bubbles caught in the iron melt and the scratches from hard sapphire particles formed by the oxidation of aluminium present in the iron ore in the course of the reduction of the iron oxides. The online identification of such surface faults by conventional optical means turns out to be difficult because the surface of the rolled steel is so rough that it scatters visible light strongly. The industrial environment (vibrations, heat, conveyor-belt speed, etc.) enforces rather large working distances and fast data-acquisition times.

Neglecting the online-operation target for the time being, we have been able to show that THz imaging with its large wavelength in the submillimetre range is blind to the natural surface roughness but provides a high sensitivity to the defects to be identified (Hasegawa *et al*. 2003). We have explored two THz reflectometry modalities which are both optimized to be sensitive to the curvature of surface features. The first is a dark-field technique employing a spatial filter in the THz beam path, which allows the detection of protrusions and dents on surfaces with high sensitivity. It cannot distinguish, however, between convex and concave shapes. This becomes possible with the second technique, which combines out-of-focus imaging with suitable beam filtering. The experiments were performed with a pulsed THz imaging system, but transfer to an optoelectronic CW THz system appears to be straightforward.

In the first dark-field approach, a THz beam is focused onto the surface of the sample, which moves along a meandering path parallel to its surface. The reflected THz beam is projected by two lenses onto a receiver, which records the signal amplitude. A circular beam stop placed between the lenses blocks the central part of the beam (Löffler *et al*. 2001, 2002). When the surface of the object is planar and normal to the beam axis, most of the reflected radiation is filtered out. If, however, the incoming beam encounters any surface features, then some radiation passes the stop and can be detected with high sensitivity.

The measurement results show that a dent with a width of 2 mm and depth of 20 μm (a protrusion of 4 mm width and 30 μm height—these parameters being determined by optical interference microscopy) can be detected with a relative contrast of more than 100 at 1 THz. The high contrast implies that features with a height (depth) of less than 1 μm should be discernible.

In spite of the impressive sensitivity, this dark-field imaging technique does not allow us to distinguish between protrusions and dents. This issue motivated develop-

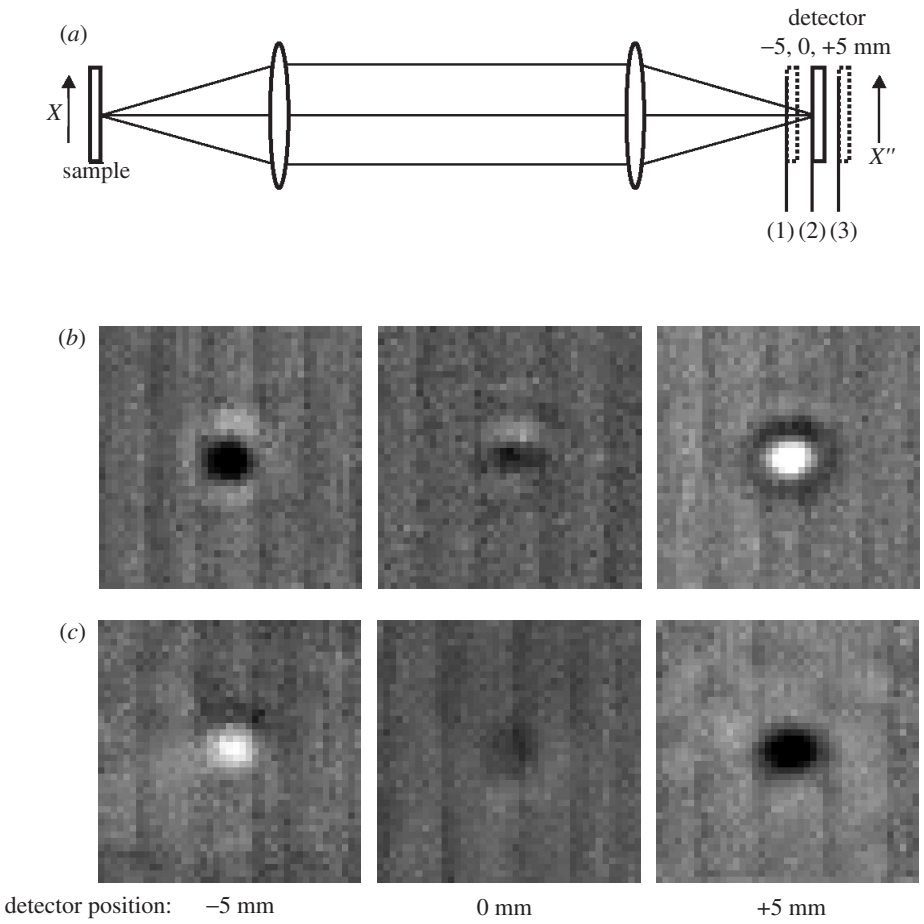

Figure 6. (*a*) Schematic of the out-of-focus detection set-up. Experimentally observed THz reflection images achieved with different detector positions for a sample containing (*b*) a dent (concave surface in centre) and (*c*) a protrusion (convex surface in centre). White colouring indicates a strong signal, black a weak signal.

ment of a second measurement technique, which does not have such a high sensitivity but introduces the ability to distinguish between convex- and concave-shaped objects.

The measurement principle is sketched in figure 6*a*. Compared with the former approach, no spatial filter is needed; a filtering effectively occurs in the detector (see Hasegawa *et al*. 2003). The key feature of this approach is that the detection occurs out of the focus of the second lens (the focus being marked as position (2)), at a certain distance (in this case, 5 mm) in front of the focus (detector position (1)) or behind it (detector position (3)). The detection principle works as follows. The focus is shifted away from the last lens, if the THz beam reflects off a concave surface (such as the centre of the dent), and it is shifted towards the lens if the surface is convex (such as the centre of the protrusion). The experimental results in figure 6*b*, *c* show that, at the detector position marked (1), these differences lead to a signal enhancement for protrusions and a decreased signal for dents. At the opposite

detector position (3), the situation is reversed. Interestingly, a detector positioned at (2) is fairly insensitive to these variations.

6. Discussion and outlook

In this paper, we have emphasized the imaging and sensing potential for THz radiation. One may ask what is necessary to bring this application area to full blossom in real-world applications. It may not be a strict prerequisite to develop THz spectroscopic databases and a better understanding of the interaction of THz radiation with matter (an understanding which, in many research areas and not only in the biomedical field, is far from being advanced), although this is clearly desirable and scientifically of high interest. The history of imaging with ultrasound shows that technical modalities can be successful even if they are not very discriminating and powerful in the spectroscopic sense. They have to bring a clear advantage, however, and must be comparatively simple, easy to handle, and provide images and sensing information in real time or close to it.

At present, we see the main obstacle for optoelectronic THz applications in imaging and sensing is the low power which these systems deliver. This argument holds for both femtosecond-laser-based systems and the CW systems discussed here. If one is not willing to spend hundreds of thousands of euros on femtosecond amplifier lasers, THz images, with the best systems available today, can only be obtained over many seconds to minutes and pixel by pixel. For this to change, it requires operation at much higher THz output powers. If a system could provide tens (or hundreds) of milliwatts and one could maintain the high detection sensitivity (at ambient temperatures) that optoelectronics provides, the opportunities for real-world applications would increase tremendously.

Several recent developments may offer new potential to achieve this goal. The advent of the quantum cascade laser which can reach into this range of output power could open the path to real-time or quasi-real-time CW THz imaging. In order to take advantage of the high sensitivity of electro-optic detection, we are seeking to develop a hybrid system consisting of a quantum cascade laser phase-locked to the difference frequency of a compact dual-colour semiconductor laser. Hopefully, quantum cascade lasers will in the future operate at room temperature or not too far below it; otherwise, this approach might suffer from the requirements for cryogenic source operation conditions.

The operation-temperature problem may be avoided if ideas of generating powerful CW THz radiation by mixing the radiation of semiconductor lasers directly in the lasers themselves turn out to be successful. These lasers could be quantum cascade lasers operating (ideally at room temperature) in the infrared spectral range or, in principle, lasers operating in the visible/near-infrared spectral regime (investigated by Professor Elsäßer at TU Darmstadt and by us).

It also remains to be seen where the return to vacuum electronics—a trend of recent years—may lead to. It is now well established that Smith–Purcell-type (Smith & Purcell 1953) emitters, based on sub-megaelectronvolt electrons in vacuum or electrons at relativistic energies forced onto curved trajectories (Carr *et al*. 2002), provide an abundance of THz radiation. The question is whether the respective machinery can be made compact and synchronized to the difference frequency of lasers for improved detectability.

Over the last one-and-a-half decades, THz research has experienced a huge upswing by the emergence of THz optoelectronics. We expect this trend to continue and to widen in scope by the integration of other technological platforms and by the application of THz research tools in a larger number of fields. A strong impact in chemistry and the biomedical–pharmaceutical area will come from the expansion of the covered frequency regime into the infrared regime, making vibrational molecular modes accessible as sources for contrast in imaging and sensing. CW THz techniques will play an important role here because of the need for narrow-band radiation in molecular spectroscopy. To most researchers in the field, it appears inevitable that industrial applications will follow, but this could well take more time (another decade or so) than anticipated by many.

7. Summary

In this paper, we have tried to give on overview of the developments concerning all-optoelectronic CW terahertz measurement systems. We have then put much emphasis on recent developments of THz radiation sources in the quest for increased output power. Another focus of the paper has been on the implementation of CW THz imaging and sensing, where we have pointed out the potential usefulness of the technique in several application areas.

The authors thank G. Strasser, TU Wien, for providing the LT-GaAs material, and V. Hock, University of Würzburg, for the Ti/Au metallization of the antennas. We are grateful for fruitful collaborations with the University of Erlangen (Professor Döhler), TU Darmstadt (Professor Elsäßer, Professor Hartnagel, Professor Meißner), the University of Osaka (Professor M. Tani) and the TERAVISION consortium concerning CW THz optoelectronics. Financial support was provided by the Deutsche Forschungsgemeinschaft and by the EU project TERAVISION. The Nippon Steel Corporation, Japan, is acknowledged for its partial support of our research on metal-surface characterization.

References

Arnone, D. D. 2000 *Opto Lasers Europe*, p. 13. (Available at http://optics.org/articles/ole.)

Arnone, D. D., Ciesla, C. & Pepper, M. 2000 *Phys. World Mag.* **13**(4), 35.

Brown, E. R., Smith, F. W. & McIntosh, K. A. 1993*a* *J. Appl. Phys.* **73**, 1480.

Brown, E. R., McIntosh, K. A., Smith, F. W., Manfra, M. J. & Dennis, C. L. 1993*b* *Appl. Phys. Lett.* **62**, 1206.

Brown, E. R., McIntosh, K. A., Smith, F. W., Manfra, M. J., Dennis, C. L. & Mattia, J. P. 1994 *Appl. Phys. Lett.* **64**, 3311.

Brown, E. R., McIntosh, K. A., Nichols, K. B. & Dennis, C. L. 1995 *Appl. Phys. Lett.* **66**, 285.

Cai, Y., Brener, I., Lopata, J., Wynn, J., Pfeiffer, L. & Federici, J. 1997 *Appl. Phys. Lett.* **71**, 2076.

Carr, G. L., Martin, M. C., McKinney, W. R., Jordan, K., Neil, G. R. & Williams, G. P. 2002 *Nature* **420**, 153.

Chen, H.-T., Kersting, R. & Cho, G. C. 2003 *Appl. Phys. Lett.* **83**, 3009–3011.

Chen, Q., Jiang, Z., Xu, G. X. & Zhang, X.-C. 2000 *Opt. Lett.* **25**, 1122.

Duerr, E. K., McIntosh, K. A. & Verghese, S. 2000 In *Proc. of Lasers and Electro-Optics (CLEO 2000), 7–12 May 2000*, pp. 382. New York: IEEE Press.

Duffy, S. M., Verghese, S., McIntosh, K. A., Jackson, A., Gossard, A. C. & Matsuura, S. 2001 *IEEE Trans. Microwave Theory Techn.* **49**, 1032.

Eckardt, M. (and 10 others) 2003 *Physica* E **17**, 629.

Ferguson, B., Wang, S., Gray, D., Abbot, D. & Zhang, X.-C. 2002 *Opt. Lett.* **27**, 1312.

Fitzgerald, A. J., Dzontoh, E., Löffler, T., Siebert, K., Berry, E., Zinovev, N. N., Miles, R. E., Smith, M. A. & Chamberlain, M. 2002 *Proc. SPIE* **4682**, 107–116.

Gu, P., Chang, F., Tani, M., Sakai, K. & Pan, C.-L. 1999 *Jpn. J. Appl. Phys. Part 2* **38**, L1246.

Han, P. Y., Cho, G. C. & Zhang, X.-C. 2000 *Opt. Lett.* **25**, 242.

Hasegawa, N., Löffler, T., Thomson, M. & Roskos, H. G. 2003 *Appl. Phys. Lett.* **83**, 3996–3998.

Herrmann, M., Tani, M. & Sakai, K. 2000 *Jpn. J. Appl. Phys.* **39**, 6254.

Hirata, A. (and 12 others) 2002 *Electron. Lett.* **38**, 798.

Hu, B. B. & Nuss, M. C. 1995 *Opt. Lett.* **20**, 1716.

Hunsche, S., Koch, M., Brener, I. & Nuss, M. C. 1998 *Opt. Commun.* **150**, 22.

Jackson, A. W., Kadow, C., Gossard, A. C., Matsuura, S., Blake, G., Duerr, E. K. & Verghese, S. 1999 In *Proc. Symp. on Non-Stoichiometric III–V Compounds, Erlangen, Germany*, p. 19.

Johnson, A. M. & Auston, D. H. 1975 *IEEE J. Quant. Electron.* **11**, 283.

Knobloch, P., Schmalstieg, K., Koch, M., Rehberg, E., Vauti, F. & Donhuijsen, K. 2001 *Hybrid and novel imaging and new optical instrumentation for biomedical applications* (ed. A.-C. Boccara & A. A. Oraevsky). *Proc. SPIE* **4434**, 245.

Köhler, R., Tredicucci, A., Beltram, F., Beere, H. E., Linfield, E. H., Davies, A. G., Ritchie, D. A., Iotti, R. C. & Rossi, F. 2002 *Nature* **417**, 156.

Kono, S., Tani, M. & Sakai, K. 2001 *Appl. Phys. Lett.* **79**, 898.

Loata, G. (and 12 others) 2003 In *Proc. IEEE Int. Conf. on Terahertz Electronics, Sendai, Japan*. New York: IEEE Press.

Löffler, T., Bauer, T., Siebert, K., Roskos, H. G., Fitzgerald, A. & Czasch, S. 2001 *Opt. Express* **9**, 616.

Löffler, T., Siebert, K., Czasch, S., Bauer, T. & Roskos, H. G. 2002 *Phys. Med. Biol.* **47**, 3847.

McIntosh, K. A., Brown, E. R., Nichols, K. B., McMahon, O. B., DiNatale, W. F. & Lyszczarz, T. M. 1995 *Appl. Phys. Lett.* **67**, 3844.

Matsuura, S., Tani, M. & Sakai, A. 1997 *Appl. Phys. Lett.* **70**, 559.

Matsuura, S., Blake, G. A., Wyss, R. A., Pearson, J. C., Kadow, C., Jackson, A. W. & Gossard, A. C. 1999 *Appl. Phys. Lett.* **74**, 2872.

Mittleman, D. M., Hunsche, S., Boivin, L. & Nuss, M. C. 1997 *Opt. Lett.* **22**, 904.

Mittleman, D. M., Gupta, M., Neelamani, R., Baraniuk, R. G., Rudd, J. V. & Koch, M. 1999 *Appl. Phys.* B **68**, 1085.

Nahata, A., Yardley, J. T. & Heinz, T. F. 1999 *Appl. Phys. Lett.* **75**, 2524.

Nahata, A., Yardley, J. T. & Heinz, T. F. 2002 *Appl. Phys. Lett.* **81**, 963.

Němec, H., Pashkin, A., Kužel, P., Khazan, M., Schnüll, S. & Wilke, I. 2001 *J. Appl. Phys.* **90**, 1303.

Pohl, P. (and 11 others) 2003 *Appl. Phys. Lett.* **83**, 4035.

Renner, F. (and 11 others) 2002 In *Proc. 4th Symp. on Non-Stoichiometric III–V Compounds, Asilomar, October 2002* (ed. P. Specht, T. R. Weatherford, P. Kiesel & S. Malzer). Physik Mikrostrukturierter Halbleiter, vol. 27, p. 59. Erlangen: Friedrich-Alexander-Universität Erlangen-Nürnberg.

Rodwell, M. J. W. (and 17 others) 2001 *IEEE Trans. Electron Devices* **48**, 2606.

Roskos, H. G. 1996 *Coherent solid-state phenomena investigated by time-resolved terahertz spectroscopy*. Habilitation thesis, Johann Wolfgang Goethe-Universität, Frankfurt-am-Main.

Segschneider, G., Jakob, F., Löffler, T., Roskos, H. G., Tautz, S., Kiesel, P. & Döhler, G. 2002 *Phys. Rev.* B **65**, 125205.

Siebe, F., Siebert, K., Leonhardt, R. & Roskos, H. G. 1999 *IEEE J. Quant. Electron.* **35**, 1731.

Siebert, K. J., Quast, H., Leonhardt, R., Löffler, T., Thomson, M., Bauer, T. & Roskos, H. G. 2002*a* *Appl. Phys. Lett.* **80**, 3003.

Siebert, K., Löffler, T., Quast, H., Thomson, M., Bauer, T., Leonhardt, R., Czasch, S. & Roskos, H. G. 2002*b* *Phys. Med. Biol.* **47**, 3743.

Smith, S. J. & Purcell, E. M. 1953 *Phys. Rev.* **92**, 1069.

Smye, S. W., Chamberlain, J. M., Fitzgerald, A. J. & Berry, E. 2001 *Phys. Med. Biol.* **46**, R101.

Stellmacher, M., Schnell, J.-P., Adam, D. & Nagle, J. 1999 *Appl. Phys. Lett.* **74**, 1239.

Sydlo, C., Sigmund, J., Hartnagel, H. L., Loata, G., Siebert, K. J. & Roskos, H. G. 2002 In *Proc. 10th IEEE Int. Conf. on Terahertz Electronics, September 2002, Cambridge, UK*. Piscataway, NJ: IEEE.

Tani, M., Sakai, K., Abe, H., Nakashima, S., Harima, H., Hangyo, M., Tokuda, Y., Kanamoto, K., Abe, Y. & Tsukada, N. 1994 *Jpn. J. Appl. Phys.* **33**, 4807.

Tani, M., Matsuura, S., Sakai, K. & Hangyo, M. 1997 *IEEE Microwave Guided Wave Lett.* **7**, 1.

Teravision 2003 Final report. (Available at http://www.teravision.org/.)

Ueda, A., Noguchi, T., Iwashita, H., Sekimoto, Y., Ishiguro, M., Takano, S., Nagatsuma, T., Ito, H., Hirata, A. & Ishibashi, T. 2003 *IEEE Trans. Microwave Theory Techn.* **51**, 1455.

van der Valk, N. C. J. & Planken, P. C. M. 2002 *Appl. Phys. Lett.* **81**, 1558.

Verghese, S., McIntosh, K. A., Calawa, S., Dinatale, W. F., Duerr, E. K. & Molvar, K. A. 1998 *Appl. Phys. Lett.* **73**, 3824.

Verghese, S., McIntosh, K. A., Duffy, S. M. & Duerr, E. K. 2001 In *Proc. NATO Advanced Research Workshop on Terahertz Sources and Systems* (ed. R. E. Miles, P. Harrison & D. Lippens). NATO Science Series, vol. 27, pp. 145–165. Dordrecht: Kluwer.

Woodward, R. M., Cole, B., Wallace, V. P., Arnone, D. D., Pye, R., Linfield, E. H., Pepper, M. & Davies, A. G. 2001 In *Proc. Conf. on Lasers and Electro-Optics (CLEO 2001)*. Trends in Optics and Photonics, vol. 56, p. 329. Washington, DC: Optical Society of America.

Wu, Q., Hewitt, T. D. & Zhang, X.-C. 1996 *Appl. Phys. Lett.* **69**, 1026.

Wynne, K. & Jaroszynski, D. A. 1999 *Opt. Lett.* **24**, 25.

Zamdmer, N., Hu, Q., McIntosh, K. A. & Verghese, S. 1999 *Appl. Phys. Lett.* **75**, 2313.

Zhao, G., Schouten, N., van der Valk, N., Wenckebach, W. T. & Planken, P. C. M. 2002 *Rev. Scient. Instrum.* **73**, 1715.

Discussion

J. Faist (*Institute of Physics, University of Neuchâtel, Switzerland*). I did not understand why you were suggesting mixing visible and THz beams inside an electro-optic sampling system.

H. G. Roskos. You want to mix a dual-colour laser that emits at its beat frequency in the THz range, and couple this THz signal to a quantum cascade laser frequency. This creates an intermediate, which you compare to the reference signal. You can now either tune the quantum cascade frequency, if you can influence that, or, perhaps more easily, let the dual-colour visible laser follow the quantum cascade laser emission. For the detection, you can either use a photoconductive technique, or possibly perform single-shot imaging with electro-optic crystals.

S. Withington (*Cavendish Laboratory, University of Cambridge, UK*). You showed very impressive measurements of iron surfaces. I think I am right in saying that there were two methods: one involved putting an aperture at the second focal plane, which picks out one spatial frequency; the other involves an out-of-focus method which is essentially a phase-retrieval technique. My question is whether you considered doing interferometry? At the second focal plane of the lens, you put two detectors, use a common reference beam, and then cross-correlate the two detected beams to get a measurement of the indentation immediately.

H. G. Roskos. In the first case, we used beam filtering in the Fourier plane, but it turns out that you do not distinguish between positive and negative curvatures. The second case was indeed an out-of-focus technique, in combination with beam filtering—the funny thing here is that the beam filtering occurs directly in the electro-optic crystal because the optical beam picks out only a small section of the THz wave that is impinging. We are indeed thinking about using different schemes in the Fourier plane, as you suggest.

S. Withington. I think that doing an interferometric measurement at the second surface would be really exciting and a good thing for someone to try.

J. Allam (*Advanced Technology Institute, University of Surrey, Guildford, UK*). Comparing the phase-resolved method, including the photomixers for generation and detection, with the earlier time-resolved method, I believe that both are coherent and both detect the average photocurrent. Would you not expect that the SNR would be essentially the same and therefore the scan time per pixel would be essentially the same?

H. G. Roskos. In hindsight this is indeed the case, but originally people argued that in the femtosecond systems there would always be a long dark time which would play an important role. It actually turns out that this is not important.

J. Allam. All things being equal, the low-temperature-grown GaAs photomixers that you use might in fact work better for your CW system. You do not have the very high instantaneous optical flux and carrier density; you therefore suffer less from screening effects, and you might be able to squeeze out more power.

H. G. Roskos. When people used silicon-on-sapphire as photomixers, the carriers were trapped for periods of nanoseconds. In femtosecond systems you do not mind because they will have recombined before the next pulse comes. However, in a CW system, this could lead to a large build-up of fixed charge and screening of the bias field, which made us very anxious initially. In fact, we have undertaken specific optical-pump THz probe measurements with our low-temperature GaAs photomixers. We find that the carriers have recombined, in all cases, after 10 ps. So screening does not play a role. But I am convinced, although we did not try it, that silicon-on-sapphire would not work for CW THz generation.

D. M. Mittleman (*Department of Electrical and Computer Engineering, Rice University, Houston, TX, USA*). I actually have almost the same question, but I am going to phrase it slightly differently! Why is your system not as fast as the femtosecond systems? It seems that the fastest pixel- or waveform-acquisition rate for the femtosecond systems is now up to about 10 000 waveforms per second, and the limiting factor is just how fast can you shake a mirror over a small optical delay. You ought to have the same sort of performance.

H. G. Roskos. It comes down in the end to how efficient the THz wave generation actually is. If you think about the photocurrents that you are driving, we would always expect 10^{-4} less power in a CW system, because the current squared should give you the emitted power. But this is not found, and I do not understand why.

G. Flinn (*TOPTICA Photonics AG, Munich, Germany*). Coming back to the semiconductor system where you have a two-colour laser and are using a broad area diode,

can you guarantee that you are going to have a similar spatial mode inside your resonator for the two wavelengths?

H. G. Roskos. Indeed, the overlap and the exact beam profiles are an issue, and the step that has still to be performed is to couple the radiation into a fibre and see how efficiently this really works. But I am very positive that this is going to work. People nowadays can integrate laser amplifiers into laser oscillators and get to single lateral and longitudinal modes at hundreds of milliwatts of power. One should be able to replicate this kind of technology in the THz field.